RSC Advances

PAPER

View Article Online
View Journal | View Issue

Cite this: *RSC Adv.*, 2020, **10**, 25046

Novel quercetin and apigenin-acetamide derivatives: design, synthesis, characterization, biological evaluation and molecular docking studies†

Daniel Isika,[a] Mustafa Çeşme,[b] Francis J. Osonga[a] and Omowunmi A. Sadik*[a]

Flavonoids exhibit essential but limited biological properties which can be enhanced through chemical modifications. In this study, we designed, synthesized, and characterized two novel flavonoid derivatives, quercetin penta-acetamide (1S3) and apigenin tri-acetamide (2S3). These compounds were confirmed using (^{1}H, ^{13}C) NMR, UV-Vis, and FT-IR characterizations. Their interaction with fish sperm DNA (FS-DNA) at physiological pH was investigated by UV-Vis and fluorescence spectrophotometry. The binding constant (K_b) for the UV-Vis experiment was found to be 1.43 ± 0.3 × 10^4 M^{-1} for 1S3 and 2.08 ± 0.2 × 10^4 M^{-1} for 2S3. The binding constants (K_{SV}) for the fluorescence quenching experiment were 1.83 × 10^4 M^{-1} and 1.96 × 10^4 M^{-1} for 1S3 and 2S3, respectively. Based on molecular modeling and docking studies, the binding affinities were found to be −7.9 and −9.1 kcal mol^{-1}, for 1S3 and 2S3, respectively. The compound–DNA docked model correlated with our experimental results, and they are groove binders. Furthermore, mutagenicity potential was examined. 1S3 and its metabolites showed no mutagenic activity for both TA98 and TA100 strains. 2S3 did not show any mutagenic activity for the strain TA 98, while its metabolites were only active at high doses. Both 2S3 and its metabolites showed mutagenic activity in the TA100 strain.

Received 23rd May 2020
Accepted 20th June 2020

DOI: 10.1039/d0ra04559d

rsc.li/rsc-advances

1. Introduction

Flavonoids are a class of polyphenolic plant metabolites structurally consisting of 15-carbons where two benzene rings are linked by a three-carbon chain to afford a C6–C3–C6 carbon skeleton. They possess anticancer,[1] antibacterial,[2] antifungal[3] and anti-inflammatory[4] properties. They exist in various classes notably flavones (such as apigenin) and flavanols (such as quercetin); structures are shown in Fig. 1. Apigenin occurs in vegetables and fruits.[5] It has anticancer,[5–7] anti-inflammatory[8] and antibacterial[9] properties. Quercetin occurs in medicinal plants, fruits and vegetables.[5] It exhibits anti-cancer,[10] antibacterial,[11] gastroprotective,[12] antiviral[13] and anti-inflammatory[14] properties.

Biological applications of flavonoids are limited by low bioavailability,[15] fast body clearance,[16] low aqueous solubility[10,17] enzyme degradation[18] and fast body metabolism.[10] To address these limitations, quercetin has been modified by the functionalization of A- and B-rings and chemical manipulation of the phenolic hydroxyl groups.[10]

Quercetin penta-phosphate and quercetin sulfonic acid are water soluble and effective in the reduction of Cr^{4+} ions.[19,20] Phosphorylated flavonoids have improved aqueous solubility and metal chelation.[20,21] They are reducing, stabilizing and capping agents in the synthesis of gold, palladium and silver nanoparticles with enhanced antimicrobial properties.[21–23]

In this study, we chemically modified quercetin and apigenin to yield quercetin- and apigenin-acetamide derivatives. The rationale is that the acetamide group comprises of a sp^3 hybridized carbon which, when incorporated into the flavonoid molecule, will induce flexibility and enhance the overall lipophilicity of the resultant derivative. The amide group would potentially increase hydrogen bonding capability and

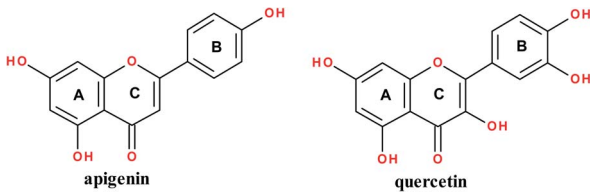

Fig. 1 Structure of apigenin and quercetin.

[a]Department of Chemistry and Environmental Science, Sensors Mechanisms Research & Technology (The SMART Center), New Jersey Institute of Technology, 161 Warren Street, University Heights, Newark, NJ 07102, USA. E-mail: sadik@njit.edu

[b]Department of Chemistry, Faculty of Art and Sciences, Kahramanmaras Sutcu Imam University, Kahramanmaras, 46040, Turkey

† Electronic supplementary information (ESI) available. See DOI: 10.1039/d0ra04559d

interaction sites, of the derivatives. The viability of these derivatives to applications in biological systems was evaluated by biological and molecular docking studies. Acetamide derivatives possess antimicrobial[24] and anti-inflammatory[25] activities. Acetamides can inhibit hepatitis C virus[26] and are possible analgesics.[27] Modafinil, levetiracetam, acetaminophen and acetazolamide are some acetamide-based drugs.

Nucleic acids are powerful tools in the recognition and monitoring of vital compounds.[28–31] The monitoring of DNA–drug interactions using spectroscopic methods is based on the fact that the fluorescence of free ligands interacts with DNA in the electronic absorption spectra.[32,33] The Ames test[34] is used to determine the mutations occurring by chemicals at the cell level.

To the best our knowledge, this is the first time the synthesis of 1S3 and 2S3 is being reported. DNA-binding of these compounds was investigated using fluorescence quenching and UV-Vis spectroscopy. The atomic details of these ligands–DNA interactions were investigated through the molecular docking method. The results based on the *in silico* DNA–ligand interaction studies show that 1S3 and 2S3 ligands are groove binders and that H-bond interactions play a principal role in the stability of these ligand–DNA complexes. This research exhibits the details of mutagenicity, the mode of binding interaction, binding affinity, main interaction forces of ligands with FS-DNA and structure of ligand–FS-DNA complex. The interaction of FS-DNA with the two synthesized compounds is significant in pharmaceutical drug discovery. Based on the *in silico* molecular docking studies, the binding score of the DNA interaction of the compounds is quite satisfactory. When the results obtained from the DNA interaction and the mutagenicity tests are evaluated, it can be concluded that these compounds can be used in biological applications and *in vivo* studies. This is after further considering that these compounds are not toxic.

2. Materials and methods

2.1 Reagents and solutions

High purity quercetin and apigenin were purchased from Indofine Chemical Company, Hillsborough, NJ, USA. Ethyl chloroacetate, dimethylformamide, thionyl chloride, lithium hydroxide monohydrate, anhydrous potassium carbonate, sodium chloride, ethyl acetate, hexane, acetone, ammonia solution, silica gel, methyl sulfoxide-d_6, sodium bicarbonate, and anhydrous sodium sulfate were purchased from Millipore Sigma (Burlington, MA, USA). All chemicals were of analytical grade and were used without further purification. Fish sperm DNA (74782) and Tris–HCl (RES3098T-B7) were supplied by Sigma-Aldrich Chemie GmbH (Germany). Ethidium bromide (EtBr) and sodium chloride (≥99.5%) were purchased from Sigma Aldrich, USA. Other chemicals and reagents purchased from Sigma or Merck and used in this work were all of the analytical grades.

2.2 Apparatus

Absorption measurements were carried out using a double-beam spectrophotometer (PerkinElmer, Lambda 25, USA) and PG spectrophotometer (T80+, UK) equipped with 1.0 cm quartz cells. Fluorescence spectra were collected on a PerkinElmer LS55 luminescence spectrophotometer. All samples were prepared in spectrophotometric grade solvents and analyzed in a 1.0 cm optical path quartz cuvette. Infrared spectra were recorded on a PerkinElmer spectrometer (Spectrum 400) equipped with ATR accessory. A pH meter (Thermo Scientific Orion Star A215 pH/conductivity benchtop) was used for the adjustment of pH values. The ^{1}H and ^{13}C NMR data were recorded on a Bruker Avance III HD 400 MHz Spectrometer.

2.3 Synthesis of the compounds

2.3.1 Triethyl 2,2′,2″-((2-(3,4-bis(2-ethoxy-2-oxoethoxy) phenyl)-4-oxo-4*H*-chromene-3,5,7-triyl)tris(oxy))triacetate (1S1). This step was achieved by using a modified literature procedure by Lee *et al.* (2007)[35] and Xia *et al.* (2010).[36]

Quercetin, 1S0, (604 mg, 2 mmol, 1 eq.) was dissolved in dry DMF (10 mL) in an oven-dried round-bottomed flask forming a brown solution. Anhydrous K_2CO_3 (2070 mg, 15 mmol, 7.5 eq.) was added and the mixture was stirred for 1 hour at room temperature. Ethyl chloroacetate (1716 mg, 14 mmol, 7 eq.) was slowly added into the reaction mixture, which was vigorously stirred at room temperature, under nitrogen gas. The progress of the reaction was monitored by TLC and the reaction was stopped after 37 hours. The final reaction mixture was filtered, and the excess solvent was removed in a rotavapor. The resultant crude solid product was dissolved in ethyl acetate and washed with 5% sodium bicarbonate, brine and finally water. The final product was purified by flash column chromatography using silica gel in (hexane/ethyl acetate/acetone, 3 : 2 : 1, v/v/v) to afford 1S1, a light yellow solid, 73% yield, $R_f = 0.22$. The structure of this compound was verified by ^{1}H and ^{13}C NMR characterizations.

1S1: δ^1H (400 MHz, DMSO-d_6): 7.82–7.67 (2H, m), 7.14–7.02 (1H, m), 6.92–6.84 (1H, m), 6.47 (1H, d, $J = 2.3$ Hz), 5.03–4.71 (10H, m), 4.24–4.08 (10H, m), 1.27–1.13 (15H, m). δ^{13}C (400 MHz, DMSO-d_6): 171.71, 168.64, 168.57, 168.40, 168.17, 167.93, 161.68, 158.58, 157.69, 151.03, 149.30, 146.60, 138.57, 123.23, 122.47, 114.65, 113.60, 108.94, 97.83, 94.83, 67.60, 65.69, 65.65, 65.20, 65.05, 60.85, 60.73, 60.63, 60.45, 14.01, 13.99, 13.91.

2.3.2 Diethyl 2,2′-((2-(4-(2-ethoxy-2-oxoethoxy)phenyl)-4-oxo-4*H*-chromene-5,7-diyl)bis(oxy))diacetate (2S1). Apigenin (540 mg, 2 mmol, 1 eq.) was dissolved in dry DMF (10 mL) in a clean oven-dried round-bottomed flask. Anhydrous potassium carbonate (1242 mg, 9 mmol, 4.5 eq.) was added and the reaction mixture was stirred at room temperature for 45 minutes. Ethyl chloroacetate (1030 mg, 0.9 mL, 8.4 mmol, 4.2 eq.) was added into the reaction mixture, which was stirred at room temperature. The progress of the reaction was monitored by TLC for 24 hours. The reaction mixture was filtered and dried; the crude solid was re-dissolved in 10 mL of ethyl acetate and washed with 5% sodium bicarbonate, brine and water (2 × 5 mL each). The organic layer was dried in anhydrous sodium sulfate prior to purification in flash column chromatography using silica gel in (hexane/ethyl acetate, 1 : 1, v/v) to yield a brown solid, 992.9 mg, 94%. $R_f = 0.16$ (hexane/ethyl acetate,

1 : 1, v/v). The structure of the intermediate product was confirmed using ^{1}H and ^{13}C NMR characterizations.

2S1: δ^1H NMR (400 MHz, DMSO-d_6) δ 7.99 (d, J = 9.0 Hz, 2H), 7.10 (d, J = 9.0 Hz, 2H), 6.93 (d, J = 2.3 Hz, 1H), 6.71 (s, 1H), 6.46 (d, J = 2.3 Hz, 1H), 4.98–4.87 (m, 6H), 4.25–4.13 (m, 6H), 1.27–1.18 (m, 9H). δ^{13}C NMR (400 MHz, DMSO-d_6) δ 175.38, 168.36, 168.27, 168.00, 161.53, 160.13, 159.66, 158.83, 158.52, 127.72, 123.63, 115.04, 109.04, 106.94, 98.11, 95.24, 65.66, 64.99, 64.73, 60.84, 60.74, 60.69, 14.01.

2.3.3 2,2′,2″-((2-(3,4-Bis(carboxymethoxy)phenyl)-4-oxo-4*H*-chromene-3,5,7-triyl)tris(oxy))triacetic acid (1S2). This step was achieved by using a modified literature procedure by Lee *et al.* (2007)[35] and Xia *et al.* (2010).[36]

1S1 (732 mg, 1 mmol, 1 eq.) was dissolved in THF/H_2O (1 : 2). Into the resultant reaction mixture, LiOH·H_2O (419.6 mg, 10 mmol, 10 eq.) was added. The reaction mixture was stirred at room temperature and the progress of the reaction was monitored by TLC for 24 hours. The excess lithium hydroxide was neutralized with 1 N HCl to afford a light-yellow precipitate which was filtered off to obtain a yellow residue. The final product was concentrated *in vacuo* and left in a line vacuum overnight to achieve 1S2 as a fine light-yellow solid, 515 mg, 87% yield. The structure was confirmed using ^{1}H NMR characterization.

1S2: δ_H (400 MHz, DMSO-d_6): 13.07 (5H, s), 7.81 (1H, d, J = 2.1 Hz), 7.74 (1H, dd, J = 8.6, 2.1 Hz), 7.06 (1H, d, J = 8.8 Hz), 6.86 (1H, d, J = 2.2 Hz), 6.45 (1H, d, J = 2.3 Hz), 4.87–4.80 (6H, m), 4.79 (2H, s), 4.70 (2H, s).

2.3.4 2,2′-((2-(4-(Carboxymethoxy)phenyl)-4-oxo-4*H*-chromene-5,7-diyl)bis(oxy))diacetic acid (2S2). 2S1 (528 mg, 1 mmol, 1 eq.) was dissolved in H_2O/THF, 2 : 1. LiOH·H_2O (252 mg, 6 mmol, 6 eq.) was slowly added into the reaction mixture at room temperature, the reaction was monitored by TLC for 14 hours. The reaction mixture was neutralized with 1 M HCl to form a light yellow precipitate. The precipitate was filtered off and purified by flash column chromatography on silica gel (methanol/water, 9 : 1, v/v). The final product was concentrated *en vacuo* and left in a line vacuum overnight to achieve 2S2, as a fine light-yellow solid, 395.4 mg, 89% yield. The structure of the product was confirmed using ^{1}H characterization.

2S2: δ_H (400 MHz, DMSO-d_6): 13.15 (3H, s), 8.06–7.97 (2H, m), 7.13–7.05 (2H, m), 6.93 (1H, d, J = 2.3 Hz), 6.75 (1H, s), 6.49 (1H, d, J = 2.3 Hz), 4.87–4.79 (6H, m).

2.3.5 2,2′,2″-((2-(3,4-bis(2-amino-2-oxoethoxy)phenyl)-4-oxo-4*H*-chromene-3,5,7-triyl)tris(oxy))triacetamide (1S3). This step was achieved by using a modified literature procedure by Li *et al.* (2012).[37]

1S2 (414.7 mg, 0.7 mmol, 1 eq.) was mixed with excess thionyl chloride in an oven-dried round-bottomed flask. The reaction mixture was vigorously stirred under reflux conditions; the reaction was monitored by TLC and was stopped after 13 hours. The reaction mixture was concentrated under reduced pressure to form a yellow powder, the acyl chloride intermediate product. This product was slowly transferred into ice-cold aqueous ammonium hydroxide. The reaction mixture was stirred at this temperature for 2 hours and at room temperature for 4 hours. The excess solvents were removed in a rotavapor followed by the purification in a flash column chromatography. The final product was a light brown solid, 329 mg, 80% yield. The products were confirmed by ^{1}H NMR, ^{13}C NMR and FT-IR characterizations.

1S3: δ_H (400 MHz, DMSO-d_6): 8.07 (1H, s), 7.88–7.65 (4H, m), 7.61 (1H, s), 7.56–7.33 (6H, m), 7.12 (1H, d, J = 8.6 Hz), 6.88 (1H, s), 6.67 (1H, s), 4.59 (8H, dd, J = 16.0, 10.2 Hz), 4.33 (2H, s).

δ^{13}C (400 MHz, DMSO-d_6): 172.93, 170.04, 169.94, 169.66, 169.57, 169.52, 168.92, 162.45, 157.67, 152.63, 149.91, 147.22, 139.17, 122.97, 122.75, 114.59, 113.71, 108.43, 98.29, 94.94, 70.24, 68.12, 67.77, 67.45, 67.03.

FT-IR: (ATR, cm^{-1}): 3411 ν(N–H), 3310 ν(N–H), 1682 ν(C=O)$_{ketone}$, 1601 ν(C=O)$_{amide}$ UV-Vis, $\lambda_{max_{nm}}$, (ε m^{-1} cm^{-1}) (DI water as solvent): 255 (1.80×10^4), 300 (9.2×10^3), 345 (1.71×10^4). Conductivity: 11.3 μS.

2.3.6 2,2′-((2-(4-(2-Amino-2-oxoethoxy)phenyl)-4-oxo-4*H*-chromene-5,7-diyl)bis(oxy))diacetamide (2S3). 2S2 (311 mg, 0.7 mmol, 1 eq.) was suspended in excess thionyl chloride in a round-bottomed flask; the reaction mixture was refluxed for 12 hours and concentrated *in vacuo* to achieve a yellow powder; the acyl chloride intermediate. The intermediate was added into an ice-cooled ammonium hydroxide. The reaction was stirred at room temperature and was monitored by TLC for 4 hours. The final product was purified in flash column chromatography to afford an orange-brown solid, 250 mg, 81% yield. The structure of the product was confirmed using ^{1}H NMR, ^{13}C NMR and FT-IR characterizations.

2S3: ^{1}H NMR (400 MHz, DMSO-d_6) δ 8.25 (1H, s), 8.02 (2H, d, J = 8.4 Hz), 7.68 (1H, s), 7.60 (2H, s), 7.45 (2H, d, J = 17.4 Hz), 7.12 (2H, d, J = 8.6 Hz), 6.92 (1H, s), 6.76 (1H, s), 6.66 (1H, d, J = 2.1 Hz), 4.64–4.51 (6H, m). ^{13}C NMR (400 MHz, DMSO-d_6) δ 176.93, 170.30, 169.88, 169.46, 162.79, 161.06, 160.97, 159.12, 158.13, 128.33, 123.84, 115.75, 108.91, 107.30, 99.17, 95.74, 68.39, 67.48, 67.20.

FT-IR: (ATR, cm^{-1}): 3391 ν(N–H), 3311 ν(N–H), 1674 ν(C=O)$_{ketone}$, 1587 ν(C=O)$_{amide}$ UV-Vis $\lambda_{max_{nm}}$, (ε m^{-1} cm^{-1}) (DMSO as solvent): 260 (1.8×10^4), 290 (1.59×10^4), 357 (2.36×10^4). Conductivity: 7.9 μS.

2.4 DNA interaction study

The stock solution of FS-DNA was prepared in a Tris–HCl buffer with a pH of 7.4 and a concentration of 50 mM then stored in the refrigerator at 4 °C for a maximum of 72 hours. In all experiments, the FS-DNA concentration was determined using the absorption band at 260 nm, and the molar absorption coefficient reported as 6600 L mol^{-1} cm^{-1} the relevant calculations were made based on this concentration.[38] To determine that FS-DNA did not contain protein impurity; the purity of the prepared stock FS-DNA solution was confirmed by the UV absorption rate (A_{260}/A_{280} > 1.8) as a result of measurements obtained at 260 and 280 nm.[39] Similarly, stock solutions of the ligands were prepared in deionized water and then diluted to desired concentrations by Tris–HCl buffer. The EtBr used in photoluminescence studies was prepared at a concentration of

3.0×10^{-3} mol L^{-1} in ethanol and used for the experiment immediately.

2.4.1 UV-Visible spectroscopy. Electronic absorption spectroscopy is one of the simplest and easiest methods for studying binding affinity in the interaction of biomolecules with ligands. In UV-Vis measurements, the absorption spectra of compounds were recorded in the 200–800 nm wavelength range. For the study of the interaction between FS-DNA and ligands, the spectra obtained by adding certain amounts of FS-DNA (0–20 μM) by titration method were recorded for each ligand solution (10 μM). All measurements were in triplicate and before the measurements of the corresponding spectrum of the mixture were taken for each sample, falcon tubes were slightly shaken and incubated for 15 minutes. The absorption spectrum obtained with the added FS-DNA was subtracted from the spectrum in the DNA–ligand measurement (the same amount of FS-DNA added) and exact spectra were gained. The intrinsic binding constant K_b was determined from the plot of [DNA]/($\varepsilon_a - \varepsilon_f$) *vs.* [DNA] graph, where [DNA] is the concentration of DNA, and the apparent absorption coefficient ε_a, ε_f, ε_b correspond to A_{obs}/[Ligand], the extinction coefficient for the free ligand compounds (1S3 and 2S3) and the extinction coefficient of the ligand compounds in the totally bound form, respectively.[40] The observed values were appointed to eqn (1), with a slope equal to $1/(\varepsilon_b - \varepsilon_f)$ and the intercept equal to $1/[K_b(\varepsilon_b - \varepsilon_f)]$. K_b was acquired from the ratio of the slope to the intercept.[39]

$$[DNA]/(\varepsilon_a - \varepsilon_f) = [DNA]/(\varepsilon_b - \varepsilon_f) + 1/[K_b(\varepsilon_b - \varepsilon_f)] \quad (1)$$

2.4.2 Fluorescence spectroscopy. Fluorescence spectroscopy is a highly sensitive and effective method for investigating the binding of ligands, particularly drugs and drug candidates, to biomacromolecules. The fluorescence quenching experiment is significant in the determination of the number of binding sites, binding constants, binding mode, and intermolecular distances of compounds with interacting potential. The interactions of DNA with the synthesized ligands were studied using a fluorescence quenching experiment. Excitation and emission slits were set at 5 and 10 nm, respectively, using a quartz cuvette with an optical path length of 1 cm. In order to investigate the binding of ligands with DNA, the FS-DNA solution was carefully mixed with ethidium bromide (EtBr), which was prepared just before the experiment, with a concentration ratio of DNA : EtBr (10 : 1) for 15 minutes at 25 °C. The binding of EtBr molecules to the double helix structure of DNA by intercalation mode causes a significant increase in the fluorescence intensity of EB. Subsequently, various amounts of ligand solutions (0–70 μM) were added to this mixture, allowing the final mixture to incubate for 15 minutes. Fluorescence spectra of the resulting final solutions were displayed in the range of 500–700 nm with an excitation wavelength of 520 nm. Fluorescence quenching efficiency was evaluated according to the following equation (Stern–Volmer equation, eqn (2)).[41]

$$I_0/I = K_{SV}[Q] + 1 \quad (2)$$

where I_0 and I are the emission intensities in the absence and presence of the quencher, K_{SV} is the quenching constant, and [Q] is the ligand (quencher) concentration. The K_{SV} values have been derived from the slopes of the plots of I_0/I *versus* [Q].

2.5 Mutagenicity assay

2.5.1 Bacterial strains. Histidine deficient (his^-) tester strains TA 98 and TA 100 of *Salmonella typhimurium* were kindly provided by J. L. Swezey, Curator, ARS Patent Culture Collection, Microbial Genomics, and Bioprocessing Research Unit, North University Street, Peoria, Illinois 61604, USA. The TA98 strain was used for the detection of frameshift mutagens while TA100 strain was used for the detection of base-pair substitution mutagens. Before their use for this assay, each strain was checked for the presence of strain-specific marker as described by Maron and Ames.[42]

2.5.2 Salmonella/microsome test (Ames). The standard plate-incorporation assay was examined with *Salmonella typhimurium* TA98 and TA100 strains both in the presence and absence of S9 mixture, according to Maron and Ames.[42] 0.5 mL of S9 mixture containing 50 μL of S9 factor per plate was used for the assay. Compounds 1S3 and 2S3 were each dissolved in distilled water to attain the concentrations of 0.40, 0.20, 0.10, 0.05 and 0.02 mg per plate. In this study, 2-AF (2-aminoflourene) was used as a positive mutagen (20 μg per plate) for both TA98 and TA100 strains in the presence of S9 mix. 4-NPD (4-nitrophenylene diamine) was used as a positive mutagen (200 μg per plate) for TA98 and TA100, per sample. The study was done with five replicate plates and all experiments were performed twice.

2.5.3 Preparation of S9. The male albino rats (*Rattus norvegicus* var. albinos) weighing 200 g were pre-treated with 80 mg kg^{-1} concentration of 3-methylcolanthrene (Oekanal, cat. no: 45794) (dissolved in sunflower seed oil) for 5 days and the S9 fraction and S9 mixture were prepared following the procedure by Maron and Ames.[42] The S9 tablets were purchased from Roche (cat. no: 1.745.425). The freshly prepared S9 fraction was distributed in 1 mL portions in small plastic tubes, which were frozen immediately and stored at −35 °C. The S9 mixture was prepared fresh for each mutagenicity assay. Each tablet was dissolved in 18 mL distilled water supplemented with 2 mL of S9 fraction.

2.5.4 Statistical significance. The statistical significance between control revertants and revertants of the treated groups was determined using the *t*-test. Between the averages of the data obtained, considering differences in the level ($p < 0.05$) were identified. The experiments were carried out in two groups, with and without S9. The average of the test results was compared with the positive and negative control groups and evaluated.

2.6 Docking and molecular modelling studies

The synthesized ligands, 1S3 and 2S3, were sketched in drawing BIOVIA Draw 2019 software and their energies minimized by Chem3D 19. Molecular modeling studies of these ligands were realized using HyperChem 8.03.[43] The molecular docking analysis was operated on the ligands against 1BNA by utilizing

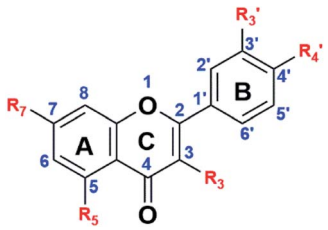

Fig. 2 General structure of the flavonoids, the intermediates and the final products. R_3, R_3', R_4', R_5 and R_7 variables are shown in Table 1.

the PyRx docking software (academic licensed version 0.9.8).[44] To evaluate the binding and interaction of the two compounds to DNA, we employed the Dickerson–Drew dodecamer (DDD) with the sequence $d(CGCGAATTCGCG)_2$ as a model system.[45] The high-resolution structure of the free DNA was downloaded from the PDB database (PDB code: 1BNA) (http://www.rcsb.org/pdb). The heteroatoms were removed from 1BNA.pdb, to remove any free ligand from the complex receptor. DNA was prepared by the addition of Kollman united atom charges, polar hydrogens, and solvation parameters. The default exhaustiveness value for both positions was set to 8 to achieve the highest level of accuracy for binding conformational analysis. Ligands were arranged by combining non-polar hydrogens and assigning the Gasteiger charge. In order to dock the synthesized ligands to DNA, a blind docking (placement) was conducted with 128 lattice points throughout the *X*, *Y*, and *Z* axes to find the binding site of complexes on DNA with a grid point range of 0.375 Å. In the next step, the center of the grid box was located at the binding site, and the second docking was performed using a cubic box with 60 × 60 × 60 dimensions. The search for best conformers was done using a Lamarckian genetic algorithm (LGA).[46] The docked complexes (1S3–DNA and 2S3–DNA) were assessed on the lowest binding energy (kcal mol^{-1}) values. The graphical depictions and related calculations of all the docking complexes were carried out and monitored using Discovery Studio 2020.

3. Results and discussion

3.1 Synthesis and NMR study of the compounds

Apigenin (4′,5,7-trihydroxyflavone) structure consists of 2-phenylchromen-4-one with three hydroxyl groups at positions 4′, 5 and 7. It has three rings: two benzene rings (ring A and B) and a pyran ring, ring C. Quercetin (2-(3,4-dihydroxyphenyl)-3,5,7-trihydroxy-4*H*-chromen-4-one) structure consist of 2-phenylchromen-4-one with five hydroxyl groups at positions 3, 3′, 4′, 5 and 7. It has three rings: two benzene rings (ring A and B) and a pyran ring, ring C; Fig. 1.

Quercetin and apigenin-acetamide derivatives were synthesized and characterized, starting from the flavonoid molecules. The structures of the intermediates and the products are shown in Fig. 2 and Table 1. The NMR characterization data conformed with the structures of both the key intermediates and the final products. The modification process was designed based on the chemistry of the phenol hydroxyl groups. These hydroxyl groups were sequentially derivatized into the desired acetamide group through an ester, carboxylic acid and acyl chloride intermediates.

The hydroxyl groups in the quercetin and apigenin molecules, S0, were converted into ester intermediates, S1, through an ether-bond formation. This step was achieved through the Williamson ether synthesis. In step 2, the ester intermediate (S1) was converted into a carboxylic acid intermediate (S2) in an ester-hydrolysis reaction. In the final step, step 3, the carboxylic acid derivative was converted into an acyl chloride, which was subsequently amidated to achieve the acetamide derivative, S3. The general steps followed are shown in Scheme 1.

Step 1 was achieved through the Williamson ether synthesis reaction. Hypothetically, this reaction proceeds through an S_N2 reaction pathway. Anhydrous potassium carbonate was used to deprotonate the flavonoid hydroxyl groups yielding poly phenoxide ions. These anions served as the nucleophile, whereas ethyl chloroacetate served as the substrate for the reaction. Excess potassium carbonate was used to ensure optimum deprotonation of the flavonoid hydroxyl groups into the corresponding nucleophiles.

The S1 derivatives were confirmed using ^1H and ^{13}C NMR characterizations. In 1S1, ^1H NMR confirmed 5 aromatic, 10 methylene (ether), 10 methylene (ester), and 15 methyl (ester) protons, by integration (Fig. S1†). 2S1 ^1H NMR integration confirmed 7 aromatic, 6 methylene (ether), 6 methylene (ester) and 9 methyl (ester) protons (Fig. S2†).

In step 2, the flavonoid-ester intermediate (S1) was converted into a flavonoid-carboxylic acid derivative (S2) through a saponification reaction. The ethoxy ($-OCH_2CH_3$) group of the flavonoid ester derivative was cleaved in an ester hydrolysis reaction. The formation of the S2 derivatives was confirmed

Table 1 R_3, R_3', R_4', R_5 and R_7 variables in Fig. 2

	R_3	R_3'	R_4'	R_5	R_7
1S0	OH	OH	OH	OH	OH
1S1	$OCH_2COOCH_2CH_3$	$OCH_2COOCH_2CH_3$	$OCH_2COOCH_2CH_3$	$OCH_2COOCH_2CH_3$	$OCH_2COOCH_2CH_3$
1S2	OCH_2COOH	OCH_2COOH	OCH_2COOH	OCH_2COOH	OCH_2COOH
1S3	OCH_2CONH_2	OCH_2CONH_2	OCH_2CONH_2	OCH_2CONH_2	OCH_2CONH_2
2S0	H	H	OH	OH	OH
2S1	H	H	$OCH_2COOCH_2CH_3$	$OCH_2COOCH_2CH_3$	$OCH_2COOCH_2CH_3$
2S2	H	H	OCH_2COOH	OCH_2COOH	OCH_2COOH
2S3	H	H	OCH_2CONH_2	OCH_2CONH_2	OCH_2CONH_2

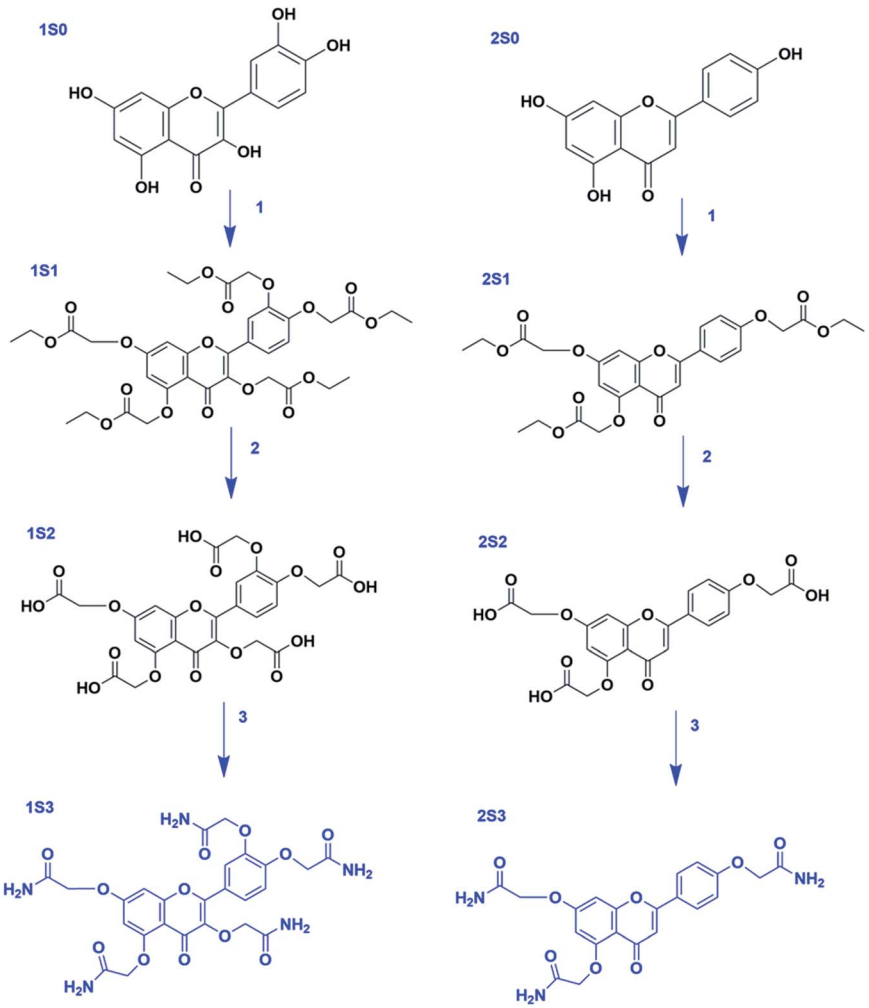

Scheme 1 Steps in the synthesis of 1S3 & 2S3 derivatives. Reagents and reaction conditions: step 1 (S0 → S1) ethyl chloroacetate, K_2CO_3 (excess), DMF, rt. Step 2 (S1 → S2) $LiOH{\cdot}H_2O$, THF/H_2O, rt. Step 3 (S2 → S3) $SOCl_2$ (excess), reflux, 75 °C; NH_4OH (excess), 0 °C – rt.

using ^{1}H NMR characterization. The ^{1}H NMR integration confirmed 5-COOH protons, 5 aromatic protons and 10 methylene protons in 1S2, Fig. S3.† In 2S2, 3-COOH protons, 7 aromatic and 6 methylene protons were confirmed by the integration of the ^{1}H NMR, Fig. S4.†

Step 3 involved the conversion of the S2 intermediate into the desired flavonoid acetamide derivative (S3). This was done by first converting the –COOH group into an acyl chloride (–COCl) by refluxing the carboxylic acid derivative with thionyl chloride. The acyl chloride intermediate, with a better leaving group, was finally converted into S3 product using an aqueous ammonium solution. The S3 product was characterized using ^{1}H & ^{13}C NMR. The ^{1}H NMR confirmed the amide, aromatic and the methylene protons.

In 1S3, 10 amide ($-CONH_2$) protons, 5 aromatic protons and 10 methylene protons were positively confirmed by the integration of the ^{1}H NMR, Fig. S5.† The additional carbons the CH_2 and the amide carbons were confirmed from the ^{13}C NMR spectrum, as shown in Fig. S6.† The 2S3 ^{1}H NMR integration confirmed 6-$CONH_2$, 7 aromatic and 6 methylene protons, Fig. S7.†

3.1.1 UV-Visible spectroscopy. The preliminary optical studies were examined by using UV-Vis spectrophotometer. Fig. 3 shows the UV-Vis absorption spectrum of 1S3 and 2S3. Both 1S3 and 2S3 have two distinct peaks and a shoulder (Fig. 3). The common characteristic absorption peaks were observed in two curves at λ_{max} 255 and 345 nm for 1S3. These peaks were detected at 260 and 335 nm for 2S3. These sharp peaks were attributed to π–π* transition within the B ring of cinnamoyl structure (the band I); the second peak (band II) may be appointed to transitions in the ring A of benzoyl structure. As we have previously reported, these characteristic peaks in the UV spectra showed absorption bands at about 257 and 374 nm for the quercetin which is the precursor of the 1S3 compound, at about 269 and 340 nm for the apigenin, the precursor of the 2S3.[19,47]

3.1.2 FTIR spectroscopy. The prominent characteristic peaks in the FT-IR spectra of the 1S3 and 2S3 derivatives are due to the amide N–H stretch. Primary amides are characterized by

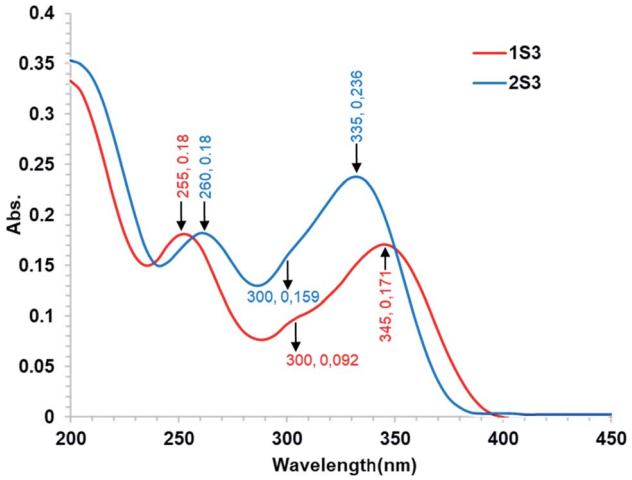

Fig. 3 Absorption spectra of 10 μmol L^{-1} 1S3 and 2S3 in Tris–HCl buffer (0.1 mol L^{-1}, pH 7.4).

two N–H absorptions. In 1S3, the amide N–H absorptions were recorded at 3411 and 3310 cm^{-1}. The corresponding N–H absorptions in 2S3 were recorded at 3391 and 3311 cm^{-1}. Additionally, the amide and ketone (C-4) C=O stretches were relatively identified in the FR-IR spectra. The ketone C=O stretching absorptions were recorded at 1682 and 1674 cm^{-1} for 1S3 and 2S3, respectively. The amide C=O stretching absorptions were recorded at 1601 and 1587 cm^{-1} for 1S3 and 2S3, respectively. The key FT-IR spectra peaks are shown in Table S1.† The FT-IR spectra of the two compounds are shown in Fig. S8.†

3.1.3 Molecular modeling studies. Geometric model structures of 1S3 and 2S3 were obtained by optimization of bond lengths, dihedral angles, and bond angles. Structures were optimized with minimum energies obtained by applying quantum chemical calculations. As shown in Fig. S9,† the ligands examined have a planar structure. The bond lengths between atoms and the bond angles are presented in detail in Tables S2 and S3.†

3.2 Compound–DNA interaction study

3.2.1 Absorption spectroscopy studies. Electronic absorption spectroscopy, one of the most employed test techniques, is extensively used in the examination of the interaction of DNA with small molecules. Commonly, the mechanism in binding small molecules to DNA through intercalative binding mode is elucidated, resulting in hypochromism and bathochromism of the resulting absorption bands.[48] When occurring electrostatic interaction between DNA and compounds, the hyperchromic effect can be seen, in which changes occur in the conformation of DNA. However, in the event of groove binding mode between DNA and compounds, the hypochromic effect can be recognized with the position of the absorption band substantially unaltered, which can be associated with the superimposing of the electronic states of the chromophore in the DNA grooves of the complex with the nitrogenous bases.[49,50]

To examine the interaction between the ligands with FS-DNA, 1S3 and 2S3 UV-Vis absorption spectra were recorded in the absence and presence of different DNA concentrations. The UV-Vis spectra of 1S3 and 2S3 in the absence and presence of FS-DNA are given in Fig. 4. In the absence of DNA, 1S3 showed two different absorbance peaks at 255 and 335 nm, respectively. As the absorption in the 255 nm band increased with the addition of DNA, the absorption at 335 nm decreased and a partial red shift was observed. Similarly, the absorption of the band at 260 nm in 2S3 increased with the addition of DNA, while the absorption of the band at 345 nm decreased and a slight redshift was observed. This can be explained by a decrease in the number of chromophores in the solution medium and conformational changes in the DNA as a result of DNA–ligand interaction. Furthermore, as a result of interaction with DNA in both compounds, approximately 300 nm isosbestic point occurred. This situation is a strong evidence[48] of the formation of a new DNA–ligand complex on the interaction of compounds and DNA affinity. Based on variations in the absorbance bands, the binding constant (K_b) for the ligand–DNA was calculated using the Benesi–Hildebrand equation (eqn (1)) and the relevant values are summarized in Table 2. The binding constant was found to be 1.43 ± 0.3 × 10^4 M^{-1} for 1S3 and 2.08 ± 0.2 × 10^4 M^{-1} for 2S3. When these values are compared with the classical intercalation agent ethidium bromide, which is known

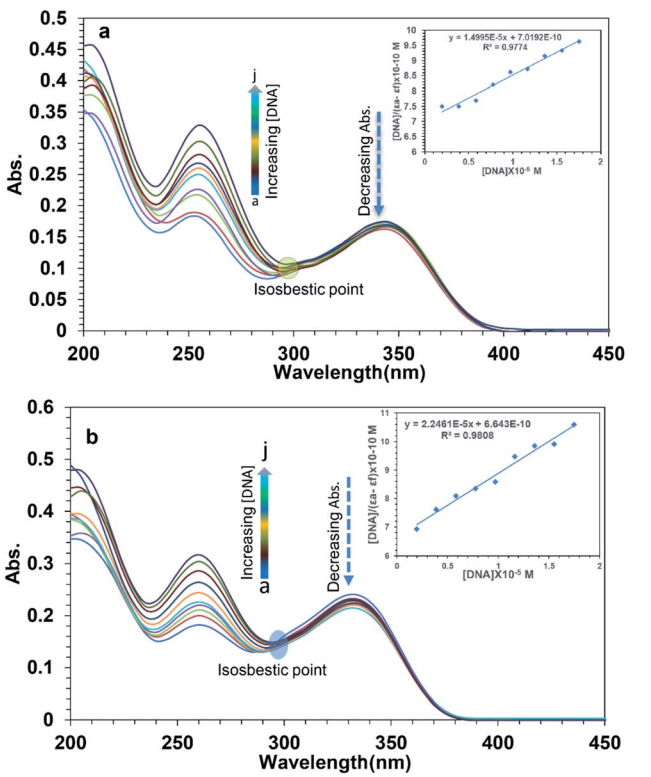

Fig. 4 Absorption spectra of 10 μmol L^{-1} 1S3 (a) and 10 μmol L^{-1} 2S3 (b) in the presence of FS-DNA at different concentrations (a: 0.0, b: 1.94, c: 3.89 d: 5.84, e: 7.78, f: 9.73, g: 11.68, h: 13.63, i: 15.58, and j: 17.52 μmol L^{-1} in Tris–HCl buffer (0.1 mol L^{-1}, pH 7.4)). The inset showing the plot of [DNA/($\varepsilon_a - \varepsilon_f$)] *versus* [DNA].

Table 2 Data obtained from spectro-analytical methods and calculations for the interaction of compounds with DNA

Property	1S3	2S3
Absorbance (nm)	335	345
K_b (M^{-1})	$1.43 \pm 03 \times 10^4$	$2.08 \pm 02 \times 10^4$
Hypochromism (%)	22.54	20.91
Isosbestic point (nm)	300	301
Shift (nm)	3	3

to interact with DNA (although the EtBr–DNA ($K_b = 1.4 \times 10^6$) complex is significantly lower than binding) it can be said that it falls within the range of groove binding[51] constant from binding modes when DNA interacts with a small molecule.

3.2.2 Fluorescence quenching studies. In order to further analyze the interaction mode of 1S3 and 2S3 with DNA, a fluorescence quenching experiment was conducted. To study this interaction, EtBr, a powerful intercalation agent well known to interact with DNA, was selected as a fluorescence indicator. EtBr has a weak fluorescence alone; however, in the presence of DNA, it shows intense fluorescence at 597 nm in stimulation at 280 nm due to its robust placement between adjacent DNA base pairs (intercalation). Therefore, the interaction of the compounds with FS-DNA can be examined in terms of changes of this characteristic peak. In the literature, it has been proven that the increased fluorescence of DNA–EtBr can be quenched by adding a second molecule through a competition between EtBr and the second molecule to bind to DNA.[31] While a significant increase in the fluorescence density of EtBr is observed upon the addition of DNA, it shows a weak fluorescence emission in solution due to the transfer of hydrogen into solution as a result of non-radiative decay from one of the amino groups of EtBr.[52] Thus, these ligands can replace EtBr by altering DNA conformation. As a result, DNA-bound EtBr molecules are transformed into their free forms in solution, quenching the fluorescence.

The fluorescence spectra of 1S3 and 2S3 in the absence and presence of FS-DNA were shown in Fig. 5. As 1S3 and 2S3 are gradually titrated into the EtBr–DNA complex, the maximum emission of the solution is reduced. This data has been validated by the interaction of the ligands with FS-DNA, which causes the formation of non-fluorescent complexes in both compounds and quenches the endogenous fluorescence. According to the eqn (2), the K_{SV} values of the compounds have been calculated to be 1.83×10^4 M^{-1} and 1.96×10^4 M^{-1} for 1S3 and 2S3, respectively. K_{SV} values calculated from the Stern–Volmer equation have lower than the values of ethidium bromide, acridine orange, and methylene blue, which are well known to have intercalation interaction with DNA.[53] Therefore, for both 1S3 and 2S3 compounds, it cannot be said that it interacts with DNA by intercalation and displaces EtBr.[54] The decrease in the fluorescence intensity of EtBr–DNA is an indication that these compounds may be partially intercalated, but this interaction is also unstable in line with the K_{SV} values obtained and the fluorescence intensity of magnitude.[55]

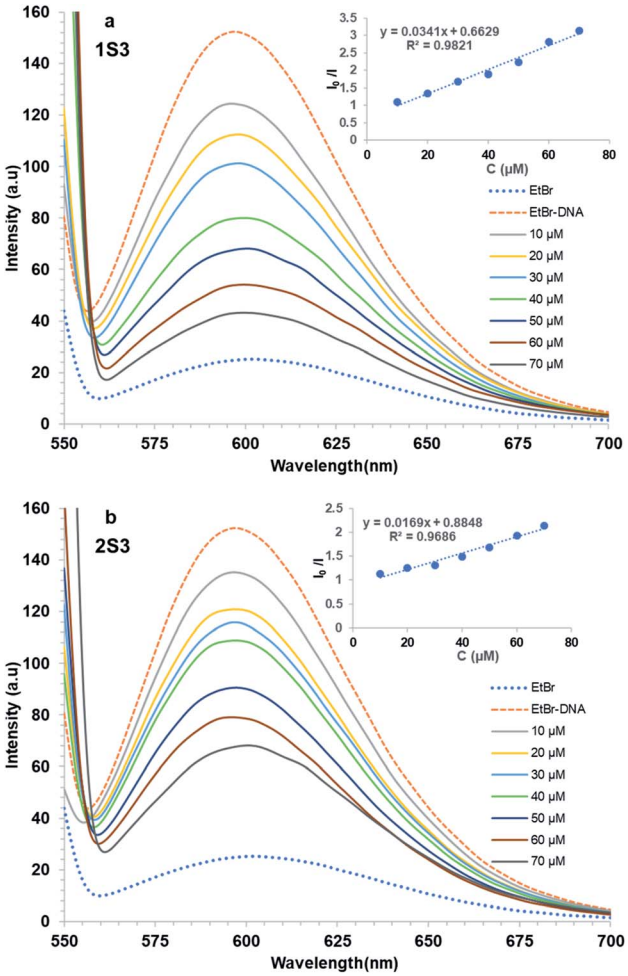

Fig. 5 Quenched Fluorescence spectra of FS-DNA bound to the EtBr system with the addition of compounds 1S3 (a) and 2S3 (b). Inset: I_0/I *versus* [DNA] (μM).

3.3 Mutagenicity properties of the compounds

Salmonella, a microsome test system, is used to detect point mutations in DNA. In this test, TA98 and TA100 strains were obtained from the LT2 ancestral strain of *Salmonella typhimurium* by a mutation *in vitro*.[56] This test was developed by Ames in 1971.[34,42,56–58] Among these strains, TA100 had base change mutation, and TA98 had frameshift mutation. Due to these mutations, these strains are unable to synthesize histidine (his^-). The principle of the experiment is based on the correction of these mutations by treating these mutated strains (TA98 and TA100) with various chemicals, *i.e.*, calculating the histidine expression frequencies of the strains (his^+). Point mutation and frameshift mutations are the basis of many genetic diseases observed in humans. There is strong evidence that it induces tumor formation in humans and animals due to base change mutations in tumor suppressor genes in both oncogenes and somatic cells.[34] Frameshift mutations occur as a result of adding/removing the base as much as 1, 2, and its multiples occurring in DNA. The mRNA synthesized from this mutated DNA molecule and the protein chain synthesized then make

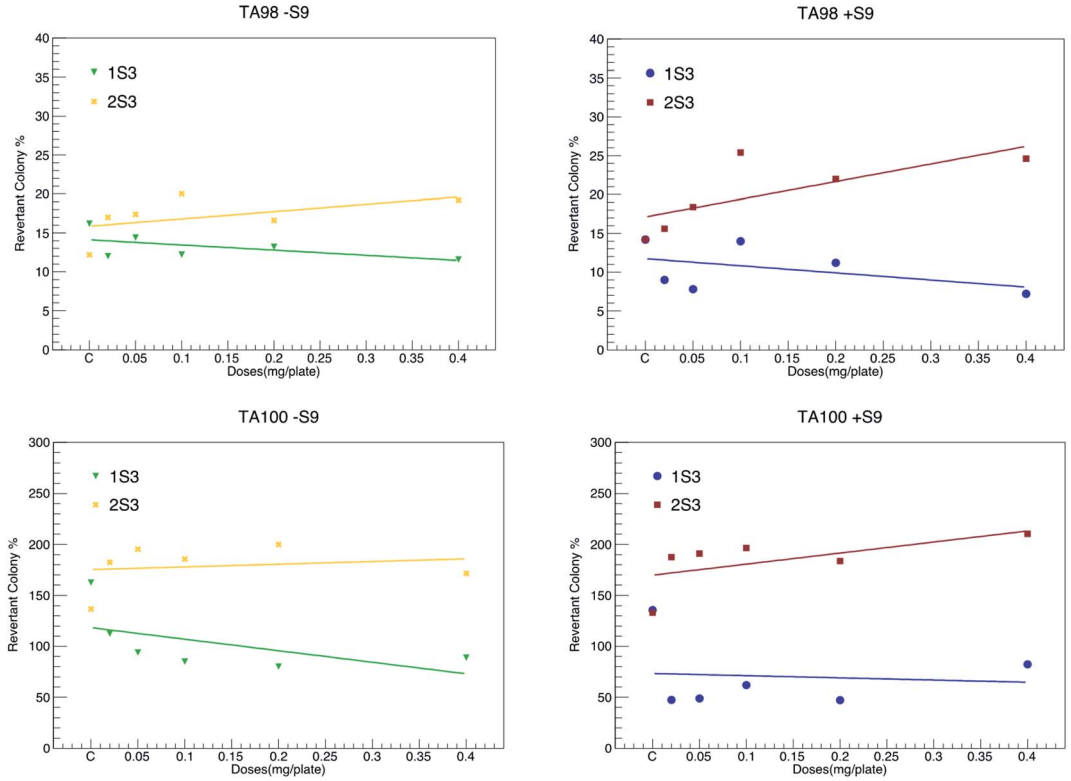

Fig. 6 Comparison graphs showing the changes in revertant colony percentages in the presence (+S9) and absence (−S9) of the metabolic activation system for TA98 and TA100 strains of compounds 1S3 and 2S3.

major changes in the amino acid sequence (in the entire chain). Therefore, if a chemical frame-shift mutation is induced, major changes occur in the protein as a result. However, since point mutations occur as a result of the structural change of one of the bases in the DNA molecule, much fewer changes occur in the mRNA synthesized from this DNA molecule and

Table 3 The mutagenicity of compounds 1S3 and 2S3 on *S. Typhimurium* TA98 and TA100 strains in the presence or absence of S9 mixture[a]

Test substances	Concentration, mg per plate	TA98		TA100	
		−S9	+S9	−S9	+S9
Spontaneous control	—	16.20 ± 1.77	14.20 ± 2.26	162.60 ± 12.23	135.80 ± 7.35
NPD	200 μg mL^{-1}	4260 ± 291.75	—	—	—
2-AF	20 μg mL^{-1}	—	2504.60 ± 397.74	—	3207.40 ± 385.93
SA	1 μg mL^{-1}	—	—	1497.2 ± 230.28	—
1S3	0.40	11.60 ± 1.63 a1b3	7.20 ± 1.68 a1b3	88.80 ± 14.07 a2b3	82.20 ± 5.37 a3b3
	0.20	13.20 ± 1.01 a1b3	11.20 ± 2.97 b3	80.20 ± 10.65 a2b3	47.00 ± 6.73 a3b3
	0.10	12.20 ± 0.66 a2b3	14.00 ± 2.60 b3	85.00 ± 7.17 a3b3	62.00 ± 4.95 a3b3
	0.05	14.40 ± 2.20 b3	7.80 ± 1.11 a2b3	94.00 ± 8.43 a3b3	48.80 ± 12.85 a2b3
	0.02	12.00 ± 1.41 a1b3	9.00 ± 0.44 a3b3	112.40 ± 3.28 a3b3	47.00 ± 7.16 a3b3
Spontaneous control		16.20 ± 1.77	14.20 ± 2.81	136.80 ± 5.95	133.20 ± 4.56
NPD		3808.40 ± 221.78	—	—	—
2-AF		—	4135.80 ± 181.49	—	3518.40 ± 385.76
SA		—	—	1506.40 ± 114.82	—
2S3	0.40	19.20 ± 2.08 b3	24.60 ± 2.11 a2b3	171.40 ± 8.55 a1b3	210.40 ± 2.31 a3b3
	0.20	16.60 ± 1.80 b3	22.00 ± 1.37 a2b3	200.00 ± 8.44 a2b3	183.60 ± 9.35 a2b3
	0.10	20.00 ± 2.25 b3	25.40 ± 1.83 a2b3	185.60 ± 7.20 a2b3	196.60 ± 15.75 a2b3
	0.05	17.40 ± 1.12 b3	18.40 ± 1.74 b3	195.40 ± 6.96 a3b3	190.80 ± 11.16 a2b3
	0.02	17.00 ± 1.00 b3	15.60 ± 2.52 b3	182.40 ± 9.15 a2b3	187.40 ± 18.93 a1b3

[a] (a) Significant from control. (b) Significant from positive control, (1) $P \leq 0.05$; (2) $P \leq 0.01$; (3) $P \leq 0.001$, NPD: 4-nitro-*o*-phenylenediamine, 2-AF: 2-aminoflourene, SA: sodium azide.

Table 4 Binding affinity energies and docking parameters of the ligand's interaction with DNA

Ligand	Binding affinity (kcal mol^{-1})	K_b (M^{-1})	Inhibition constant at 298.15 K (μM)
1S3	−7.9	1.74×10^4	1.92
2S3	−9.1	2.23×10^4	2.34

subsequently the synthesized protein molecule. Compound 1S3 did not cause any detectable increase in the number of revertant colonies in both TA98 and TA100 strains, both in the presence (+S9 mixture) and the absence of the metabolic activation system (−S9 mixture). This shows that both the 1S3 and its metabolites do not have any mutagenic activity.

Our study reveals that compound 2S3 did not cause an increase in the number of revertant colonies in the absence of a metabolic activation system for the TA98 strain. However, this compound caused a statistically significant increase in the number of revertant colonies in high doses (0.40, 0.20 and 0.10 mg per plate) in the presence of metabolic activation system.[34] In addition, 2S3 significantly increased the number of revertant colonies for TA100 strain both in the presence and the absence of the activation system. This shows that both the 2S3 and its metabolites are potentially mutagenic for the TA100 strain at high doses. It is evident that strain TA98 shows frameshift mutation and strain TA100 shows base change mutation.[58] In summary, 1S3 does not have any mutagenic potential in both TA98 and TA100 strains. Compound 2S3 does not show any mutagenic activity in the TA98 strain; however, its metabolites have a mutagenic potential at high doses. In addition, both the 2S3 itself and its metabolites have mutagenic activity in the TA100 strain. The values of both compounds are given in detail in Fig. 6 and Table 3. According to the data that we obtained from this study, we can conclude that compound 1S3 by itself and its metabolites are not mutagenic because they do not cause frameshifts and point mutations. On the other hand, compound 2S3 by itself does not induce the frame-shift mutation, but it induces metabolites at high doses. It further induces the point mutation of both 2S3 itself and its metabolites. Therefore, we can conclude that it has mutagenic potential.

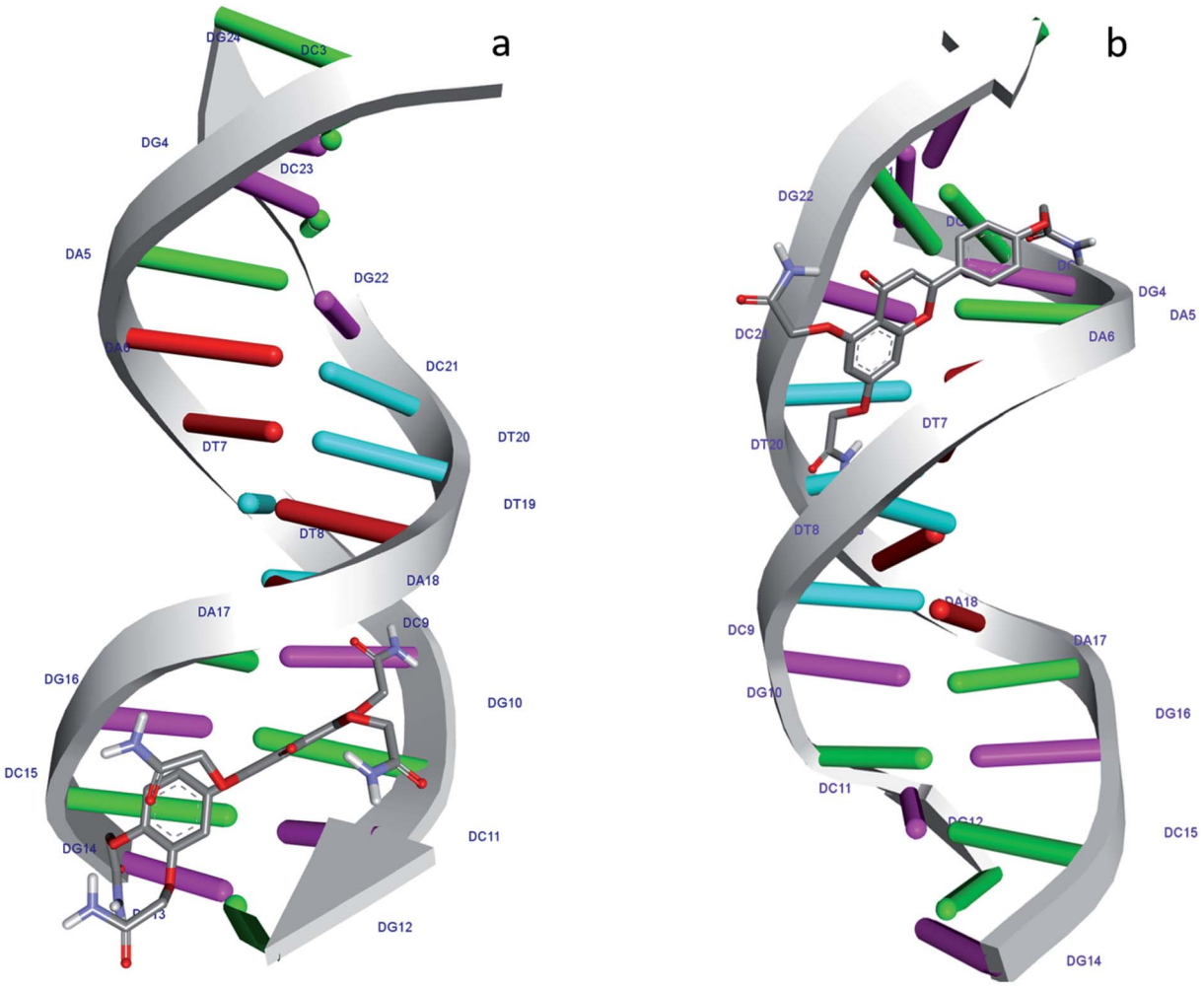

Fig. 7 Molecular docked structure of 1S3 (a) and 2S3 (b) complexed with DNA. Surface representation showing the binding of 1S3 and 2S3 with the dodecamer duplex sequence, d(CGCGAATTCGCG)$_2$ (PDB ID: 1BNA).

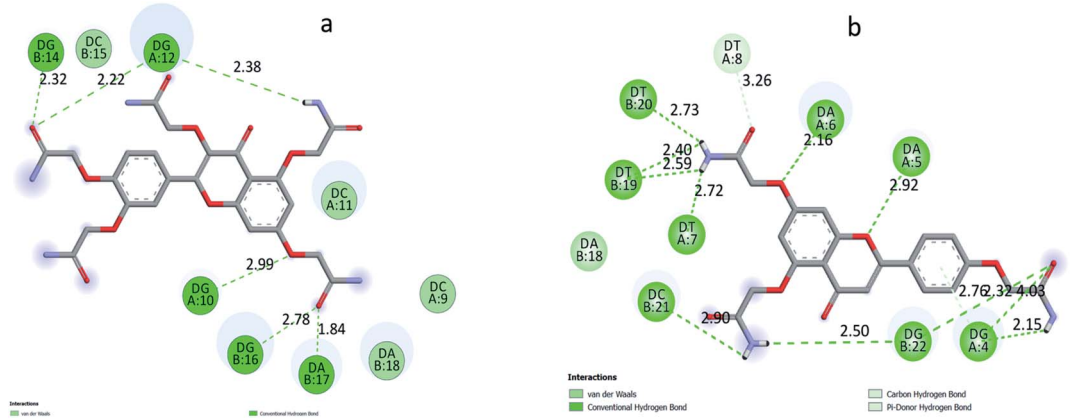

Fig. 8 2D plot of interaction between the 1S3 (a) and 2S3 (b) with the dodecamer duplex sequence, d(CGCGAATTCGCG)$_2$ (PDB ID: 1BNA).

3.4 Molecular docking studies

Molecular docking studies have gained an increasing interest in the research of the binding interaction mechanisms of biological macromolecules with small molecules. Molecular docking is a valuable technique in rational drug design to predict the most stable structure, binding tendency, and binding mode of the receptor–ligand complex so that interaction details can be better recognized and examined during new drug discovery and development process. This method is often used as virtual search tools in crucial steps of drug design and development. Molecular docking studies have been conducted to find the preferred location of ligands on DNA. In general, the more negative the binding energy resulting from the interaction, the more stable the small molecule and the complex formed by the DNA, the stronger the interaction between the small molecule and the DNA.[30] The docking energy values and inhibition constants of the ligands during their interaction with DNA are given in Table 4.

According to the docking models, 1S3 binds to the major groove of DNA, while 2S3 binds to the minor groove. The binding affinities were found to be −7.9 and −9.1 kcal mol^{-1} according to the best pose conditions-for the 1S3 and 2S3, respectively. These scores relate to the minimum binding energy and the maximum

Table 5 Interactions types and distances of 1S3 and 2S3 with DNA complexes

	Interactions	Distance	Bonding types	From	To
1S3–DNA complex	A:DG10:H3 – :1S3:O35	2.98657	Conventional H bond	A:DG10:H3	:1S3:O35
	A:DG12:H22 – :1S3:O30	2.21828	Conventional H bond	A:DG12:H22	:1S3:O30
	B:DG14:H3 – :1S3:O30	2.32444	Conventional H bond	B:DG14:H3	:1S3:O30
	B:DG16:H22 – :1S3:O39	2.77904	Conventional H bond	B:DG16:H22	:1S3:O39
	B:DA17:H3 – :1S3:O39	1.84249	Conventional H bond	B:DA17:H3	:1S3:O39
	:1S3:H57 – :1S3:O25	2.51626	Conventional H bond	:1S3:H57	:1S3:O25
	:1S3:H60 – :1S3:O26	2.439	Conventional H bond	:1S3:H60	:1S3:O26
	:1S3:H47 – A:DG12:OP1	2.37572	Conventional H bond	:1S3:H47	A:DG12:OP1
	:1S3:H48 – :1S3:O11	2.24041	Conventional H bond	:1S3:H48	:1S3:O11
	Interactions	Distance	Types	From	To
2S3–DNA complex	:2S3:H42 – A:DG4:O4′	2.15093	Conventional H bond	:2S3:H42	A:DG4:O4′
	:2S3:H50 – A:DT7:O2	2.71946	Conventional H bond	:2S3:H50	A:DT7:O2
	:2S3:H50 – B:DT19:O2	2.59064	Conventional H bond	:2S3:H50	B:DT19:O2
	:2S3:H51 – B:DT19:O2	2.40101	Conventional H bond	:2S3:H51	B:DT19:O2
	:2S3:H51 – B:DT20:O2	2.73073	Conventional H bond	:2S3:H51	B:DT20:O2
	:2S3:H46 – B:DG22:OP1	2.49963	Conventional H bond	:2S3:H46	B:DG22:OP1
	:2S3:H47 – :2S3:O11	1.92188	Conventional H bond	:2S3:H47	:2S3:O11
	:2S3:H47 – B:DC21:O3′	2.90098	Conventional H bond	:2S3:H47	B:DC21:O3′
	A:DG4:H22 – :2S3:O22	2.92642	Conventional H bond	A:DG4:H22	:2S3:O22
	A:DG4:H3 –:2S3:O22	2.4405	Conventional H bond	A:DG4:H3	:2S3:O22
	A:DA5:H3 – :2S3:O7	2.92123	Conventional H bond	A:DA5:H3	:2S3:O7
	A:DA6:H3 – :2S3:O28	2.16167	Conventional H bond	A:DA6:H3	:2S3:O28
	B:DG22:H22 – :2S3:O22	2.32328	Conventional H bond	B:DG22:H22	:2S3:O22
	A:DT8:C5′ – :2S3:O32	3.25681	Carbon–H bond	A:DT8:C5′	:2S3:O32
	A:DG4:H22 – :2S3	2.75747	Pi-donor-H bond	A:DG4:H22	:2S3

docking cluster. These results are compatible with the spectroscopic results obtained. In addition, docking studies have shown that H-bond interactions play the main role in the stability of ligand–DNA complexes. The energetically most convenient conformation of the docked pose of DNA–ligand complexes is depicted in Fig. 7 as a 3D. When the 2D plot of the interaction between DNA with 1S3 and 2S3 is examined (Fig. 8), for 1S3, DNA appears to have 6 different H-bond interactions with both A and B chain. Considering the nucleotide-binding and the molecular structure of 1S3, it is seen that the hydrogen bonds formed in the 1S3–DNA complex occur *via* the nucleotides of the guanine and adenine and the oxygen in the amide groups of the compound. For 2S3, a significant change has occurred in the conformation of the molecule to exhibit the ability to bind along the minor groove, and this conformational change is closely related to the structure of the DNA minor groove. Besides, this situation can be described as an important indication that the DNA–2S3 complex is formed. The interaction between the ligand and DNA for the DNA–2S3 complex occurred *via* amide groups attached to the aromatic ring, as in 1S3. However, apart from the conventional hydrogen bond, carbon–H bond and Pi-donor-H bond interactions were observed. For the 1S3–DNA and 2S3–DNA complexes, the data showing the bonds, bond types, and bond lengths formed between the nucleotides and ligands are summarized in Table 5. For the 1S3–DNA and 2S3–DNA complexes, the docked model illustrations are given in detail in the ESI, Fig. S10–S19.†

4. Conclusion

In the present study, we have successfully synthesized two new flavonoid acetamide derivatives namely: 2,2′,2″-((2-(3,4-bis(2-amino-2-oxoethoxy)phenyl)-4-oxo-4*H*-chromene-3,5,7-triyl)tris (oxy))triacetamide (1S3) and 2,2′-((2-(4-(2-amino-2-oxoethoxy) phenyl)-4-oxo-4*H*-chromene-5,7-diyl)bis(oxy))diacetamide (2S3). To the best our knowledge, this is the first time the synthesis of these derivatives is being reported. DNA-binding of these compounds/ligands was investigated using fluorescence quenching and UV-Vis spectroscopy. Furthermore, the atomic details of these ligands–DNA interactions were investigated using the molecular docking method. The results based on the *in silico* DNA–ligand interaction studies show that 1S3 and 2S3 ligands are groove binders and that H-bond interactions have played a principal role in the stability of these ligand–DNA complexes. The present research exhibits the details of the mode of binding interaction, binding affinity, main interaction forces of ligands with FS-DNA and structure of ligand–FS-DNA complex. The flavonoid acetamide derivatives were tested for mutagenicity effect. Therefore, the results obtained from this study, focusing on the interaction mechanisms of flavonoid acetamide-derived ligands on FS-DNA, both experimental and molecular docking, will present useful information to entirely comprehend the mechanism of action and pharmacokinetics of these flavonoid derivatives.

Conflicts of interest

The authors declare no conflicts of interest.

Acknowledgements

The authors acknowledge the National Science Foundation Grant # IOS-1543944 and the Bill & Melinda Gates Foundation for funding.

References

1 W. Ren, Z. Qiao, H. Wang, L. Zhu and L. Zhang, *Med. Res. Rev.*, 2003, **23**, 519–534.
2 T. P. T. Cushnie and A. J. Lamb, *Int. J. Antimicrob. Agents*, 2011, **38**, 99–107.
3 R. M. De Conti Lourenço, P. Da Silva Melo and A. B. A. De Almeida, in *Antifungal Metabolites from Plants*, Springer-Verlag, Berlin Heidelberg, 2013, pp. 283–300.
4 A. García-Lafuente, E. Guillamón, A. Villares, M. A. Rostagno and J. A. Martínez, *Inflammation Res.*, 2009, **58**, 537–552.
5 A. N. Panche, A. D. Diwan and S. R. Chandra, *J. Nutr. Sci.*, 2016, **5**(1), DOI: 10.1017/jns.2016.41.
6 T. Der Way, M. C. Kao and J. K. Lin, *J. Biol. Chem.*, 2004, **279**, 4479–4489.
7 A. Kowalczyk, A. Bodalska, M. Miranowicz and K. Karłowicz-Bodalska, *Adv. Clin. Exp. Med.*, 2017, **26**, 1143–1146.
8 X. Zhang, G. Wang, E. C. Gurley and H. Zhou, *PLoS One*, 2014, **9**(9), e107072.
9 R. Liu, H. Zhang, M. Yuan, J. Zhou, Q. Tu, J. J. Liu and J. Wang, *Molecules*, 2013, **18**, 11496–11511.
10 A. Massi, O. Bortolini, D. Ragno, T. Bernardi, G. Sacchetti, M. Tacchini and C. De Risi, *Molecules*, 2017, **22**, 1270.
11 F. A. Ramos, Y. Takaishi, M. Shirotori, Y. Kawaguchi, K. Tsuchiya, H. Shibata, T. Higuti, T. Tadokoro and M. Takeuchi, *J. Agric. Food Chem.*, 2006, **54**, 3551–3557.
12 A. V. Anand David, R. Arulmoli and S. Parasuraman, *Pharmacogn. Rev.*, 2016, **10**, 84–89.
13 J. Johari, A. Kianmehr, M. R. Mustafa, S. Abubakar and K. Zandi, *Int. J. Mol. Sci.*, 2012, **13**, 16020–16045.
14 N. Rani, L. P. T. Velan, S. Vijaykumar and A. Arunachalam, *Chin. J. Integr. Med.*, 2015, **9**, 1–16.
15 M. Russo, C. Spagnuolo, I. Tedesco, S. Bilotto and G. L. Russo, *Biochem. Pharmacol.*, 2012, **83**, 6–15.
16 W. Wang, C. Sun, L. Mao, P. Ma, F. Liu, J. Yang and Y. Gao, *Trends Food Sci. Technol.*, 2016, **56**, 21–38.
17 D. Patel, S. Shukla and S. Gupta, *Int. J. Oncol.*, 2007, **30**, 233–245.
18 M. Saibu, S. Sagar, I. Green, F. Ameer and M. Meyer, *Anticancer Res.*, 2014, **34**, 4077–4086.
19 V. A. Okello, S. Mwilu, N. Noah, A. Zhou, J. Chong, M. T. Knipfing, D. Doetschman and O. A. Sadik, *Environ. Sci. Technol.*, 2012, **46**, 10743–10751.
20 F. J. Osonga, J. O. Onyango, S. K. Mwilu, N. M. Noah, J. J. J. J. Schulte, M. An and O. A. Sadik, *Tetrahedron Lett.*, 2017, **58**, 1474–1479.
21 F. J. Osonga, I. Yazgan, V. Kariuki, D. Luther, A. Jimenez, P. Le and O. A. Sadik, *RSC Adv.*, 2016, **6**, 2302–2313.
22 F. J. Osonga, S. Kalra, R. M. Miller, D. Isika and O. A. Sadik, *RSC Adv.*, 2020, **10**, 5894–5904.

23 F. J. Osonga, A. A. A. Akgul, I. Yazgan, A. A. A. Akgul, R. Ontman, V. M. M. Kariuki, G. B. Eshun and O. A. Sadik, *RSC Adv.*, 2018, **8**, 4649–4661.
24 R. V. Patel, P. Kumari, D. P. Rajani and K. H. Chikhalia, *Med. Chem. Res.*, 2013, **22**, 195–210.
25 O. Kouatly, A. Geronikaki, C. Kamoutsis, D. Hadjipavlou-Litina and P. Eleftheriou, *Eur. J. Med. Chem.*, 2009, **44**, 1198–1204.
26 S. Harper, B. Pacini, S. Avolio, M. Di Filippo, G. Migliaccio, R. Laufer, R. De Francesco, M. Rowley and F. Narjes, *J. Med. Chem.*, 2005, **48**, 1314–1317.
27 P. S. Nayak, B. Narayana, B. K. Sarojini, K. Hegde and K. S. Shashidhara, *Med. Chem. Res.*, 2014, **23**, 4280–4294.
28 K. Al-Jorani, A. Rüther, M. Martin, R. Haputhanthri, G. B. Deacon, H. L. Li and B. R. Wood, *Sensors*, 2018, **18**(12), 4297.
29 R. Hajian, P. Hossaini, Z. Mehrayin, P. M. Woi and N. Shams, *J. Pharm. Anal.*, 2017, **7**, 176–180.
30 J. H. Shi, K. L. Zhou, Y. Y. Lou and D. Q. Pan, *Spectrochim. Acta, Part A*, 2018, **193**, 14–22.
31 N. Shahabadi, F. Shiri and S. Hadidi, *Spectrochim. Acta, Part A*, 2019, **219**, 195–201.
32 R. K. Gilpin and C. S. Gilpin, *Anal. Chem.*, 2011, **83**, 4489–4507.
33 R. B. Silverman and M. W. Holladay, *The Organic Chemistry of Drug Design and Drug Action*, Elsevier, 3rd edn, 2014.
34 B. N. Ames, J. McCann and E. Yamasaki, *Mutat. Res., Environ. Mutagen. Relat. Subj.*, 1975, **31**, 347–363.
35 K. Lee, J. H. Lee, S. K. Boovanahalli, Y. Jin, M. Lee, X. Jin, J. H. Kim, Y.-S. Hong and J. J. Lee, *J. Med. Chem.*, 2007, **50**, 1675–1684.
36 Y. Xia, M.-S. Won, J.-E. Kang, S.-K. Park, K.-H. Lee, H.-M. Kim and K. Lee, *Bull. Korean Chem. Soc.*, 2010, **31**, 3826–3829.
37 T. Li, G. Liu, H. Li, X. Yang, Y. Jing and G. Zhao, *Bioorg. Med. Chem.*, 2012, **20**, 2316–2322.
38 J. Lakshmipraba, S. Arunachalam, R. V. Solomon, P. Venuvanalingam, A. Riyasdeen, R. Dhivya and M. A. Akbarsha, *J. Biomol. Struct. Dyn.*, 2015, **33**, 877–891.
39 M. E. Reichmann, S. A. Rice, C. A. Thomas and P. Doty, *J. Am. Chem. Soc.*, 1954, **76**, 3047–3053.
40 V. L. Elena and L. E. Vîjan, *Optoelectron. Adv. Mater., Rapid Commun.*, 2009, **3**, 60–64.
41 L. Liu, C. Zhang, Y. Yu and F. Chen, *Microchim. Acta*, 2018, **185**(11), 514.
42 D. M. Maron and B. N. Ames, *Mutat. Res., Environ. Mutagen. Relat. Subj.*, 1983, **113**, 173–215.
43 *M. M. 8. HyperChem™ Professional Chemistry Software*.
44 S. Dallakyan and A. J. Olson, in *Global Food Security Governance*, ed. J. E. Hempel, C. H. Williams and C. C. Hong, Springer New York, New York, NY, 2015, vol. 1263, pp. 243–250.
45 H. R. Drew, R. M. Wing, T. Takano, C. Broka, S. Tanaka, K. Itakura and R. E. Dickerson, *Proc. Natl. Acad. Sci. U. S. A.*, 1981, **78**, 2179–2183.
46 S. K. Tripathi, R. Muttineni and S. K. Singh, *J. Theor. Biol.*, 2013, **334**, 87–100.
47 B. Li, D. H. Robinson and D. F. Birt, *J. Pharm. Sci.*, 1997, **86**, 721–725.
48 M. Sirajuddin, S. Ali and A. Badshah, *J. Photochem. Photobiol., B*, 2013, **124**, 1–19.
49 X. Xu, D. Wang, X. Sun, S. Zeng, L. Li and D. Sun, *Thermochim. Acta*, 2009, **493**, 30–36.
50 A. Shah, E. Nosheen, S. Munir, A. Badshah, R. Qureshi, Z. U. Rehman, N. Muhammad and H. Hussain, *J. Photochem. Photobiol., B*, 2013, **120**, 90–97.
51 J. H. Shi, J. Chen, J. Wang and Y. Y. Zhu, *Spectrochim. Acta, Part A*, 2015, **136**, 443–450.
52 A. Jamshidvand, M. Sahihi, V. Mirkhani, M. Moghadam, I. Mohammadpoor-Baltork, S. Tangestaninejad, H. Amiri Rudbari, H. Kargar, R. Keshavarzi and S. Gharaghani, *J. Mol. Liq.*, 2018, **253**, 61–71.
53 S. Nafisi, A. A. Saboury, N. Keramat, J.-F. F. Neault and H.-A. A. Tajmir-Riahi, *J. Mol. Struct.*, 2007, **827**, 35–43.
54 Y. Sha, X. Chen, B. Niu and Q. Chen, *Chem. Biodiversity*, 2017, **14**(10), e1700133.
55 C. Gan, X. Huang, J. Zhan, X. Liu, Y. Huang and J. Cui, *Spectrochim. Acta, Part A*, 2020, **227**, 117525.
56 L. Snyder, J. Peters, W. Champness and T. Henkin, *Molecular Genetics of Bacteria*, 2012.
57 K. Mortelmans and E. Zeiger, *Mutat. Res.*, 2000, **455**, 29–60.
58 A. Kayraldiz, F. F. Kaya, S. Canimoğlu and E. Rencüzoğullari, *Ann. Microbiol.*, 2006, **56**, 129–133.